

A large energy-gap oxide topological insulator based on the superconductor BaBiO₃

Binghai Yan,^{1,2,3,*} Martin Jansen,¹ and Claudia Felser¹

¹Max Planck Institute for Chemical Physics of Solids, D-01187 Dresden, Germany

²Max Planck Institute for the Physics of Complex Systems, D-01187 Dresden, Germany

³Institute for Inorganic and Analytical Chemistry,

Johannes Gutenberg University of Mainz, 55099 Mainz, Germany

Mixed-valent perovskite oxides based on BaBiO₃ [1, 2] (BBO) are, like cuprates, well-known high- T_c superconductors. Recent *ab initio* calculations [10] have assigned the high- T_c superconductivity to a correlation-enhanced electron-phonon coupling mechanism, stimulating the prediction and synthesis of new superconductor candidates among mixed-valent thallium perovskites [4–6]. Existing superconductivity has meant that research has mainly focused on hole-doped compounds, leaving electron-doped compounds relatively unexplored. Here we demonstrate through *ab initio* calculations that BBO emerges as a topological insulator [7–10] (TI) in the electron-doped region, where the spin-orbit coupling (SOC) effect is significant. BBO exhibits the largest topological energy gap of 0.7 eV among currently known TI materials [11], inside which Dirac-type topological surface states (TSSs) exit. As the first oxide TI, BBO is naturally stable against surface oxidization and degrading, different from chalcogenide TIs. An extra advantage of BBO lies in its ability to serve an interface between the TSSs and the superconductor for the realization of Majorana Fermions [12].

The parent compound BBO crystallizes in a mononclinic lattice that is distorted from the perovskite structure, and this distortion is attributed to the coexistence of two valence states, Bi³⁺ ($6s^2$) and Bi⁵⁺ ($6s^0$), due to charge disproportion of the formal Bi⁴⁺. Octahedral BiO₆ breathes out and in for Bi³⁺ and Bi⁵⁺, respectively [9]. Under hole-doping conditions, such as in Ba_{1-x}K_xBiO₃ ($x \sim 0.4$) [2, 14] and BaBi_{1-x}Pb_xO₃ ($x \sim 0.3$) [1, 15], the breathing distortion is suppressed, resulting in a simple perovskite lattice [16] in which superconductivity emerges. The O-breathing phonon mode of BiO₆ is believed to result in the pairing of superconducting electrons in the Bardeen-Cooper-Schrieffer (BCS) framework [10]. In addition to the breathing distortion, undoped BBO also presents extra O-tilting distortions [9], finally resulting in a mononclinic phase. However, in ref. 10 and earlier work [11, 13, 19], SOC was not taken into account in the theoretical study, since the electronic states in the superconducting (hole-doped) region mainly result from Bi-6s and O-2p orbitals whose SOC effect is usually negligible.

By including the SOC effect in density-functional theory calculations of the BBO band structure, we discovered a band inversion between the first (Bi-6s state) and second (Bi-6p state) conduction bands, which is stable against lattice distortions. This inversion indicates that BBO is a three-dimensional (3D) TI with a large indirect energy gap of 0.7 eV when doped by electrons instead of holes. The band structure of ideal cubic BBO (Fig. 1A) reveals that the conduction bands are modified dramatically when SOC is included due to the presence of the Bi-6p states. The first conduction band crossing the Fermi energy (E_F) has a considerable Bi-6s contribution over the whole Brillouin zone, except at the R momentum

point where the Bi-6p contribution is dominant. Without SOC there is a zero energy gap at R because of the degeneracy of the p states. When the SOC is included, the $|p, j = 3/2\rangle$ and $|p, j = 1/2\rangle$ states split, which results in the large indirect energy gap of 0.7 eV in the vicinity of the R point. Here, the Bi-6s state lies above the Bi-6p states, causing band inversion around the energy gap (Fig. 1A). Unlike bulk HgTe [20, 21], a well-known TI, this inversion occurs between the $|s, j = 1/2\rangle$ state and the $|p, j = 1/2\rangle$ state, rather than $|p, j = 3/2\rangle$ state. Since the Bi atom is the inversion centre of the perovskite lattice, the $|s, j = 1/2\rangle$ and $|p, j = 1/2\rangle$ states have “+” and “-” parities, respectively. Thus, a TI state can be obtained if E_F is shifted up into this energy gap. The parities of all the valence bands below this gap were also calculated at all time-reversal invariant momenta, Γ (0 0 0), X (0.5 0 0), M (0.5 0.5 0), and R (0.5 0.5 0.5), which yielded Z_2 topological invariants (1;111), confirming the topological nontrivial feature according to Fu and Kane’s [22] parity criteria. At a doping rate of one electron per formula unit, E_F shifts inside the s - p inversion gap, and all the Bi⁵⁺ ions become Bi³⁺. Consequently, a cubic phase appears when the BiO₆ breathing distortion is suppressed, similar to the hole-doping case [16]. The new cubic lattice is found to expand only slightly in comparison to the undoped lattice because the Bi³⁺-O bond is longer than the Bi⁵⁺-O bond due to the localized Bi-6s orbital, while the band inversion is unaffected.

To illustrate the TSSs, we calculated the surface band structure using a slab model. As an example, we take the surface to be oriented along the (001) direction on which the bulk R point is projected onto the \bar{M} point of the surface Brillouin zone. The slab is thirty BBO units thick with the outermost atomic layers being Ba-O. The TSSs,

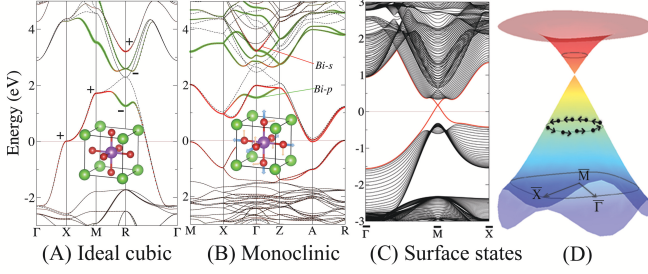


FIG. 1: Band structures of bulk BiBaO_3 of the (A) ideal cubic and (B) monoclinic structures. The solid and dashed lines represent results with and without SOC, respectively, while the red and green dots indicate the Bi- s and Bi- p states, respectively. The parities are labelled in A. The Fermi energy is set to zero. The lattice structures are shown in the insets, where Bi is shown in purple, O in red, and Ba in green. The monoclinic structure includes four formula units of BBO with O-breathing (blue arrows) and O-tilting (yellow arrows) distortions from a cubic lattice. (C) The surface states of an electron-doped BiBaO_3 surface normalized along the (001) direction. The red lines highlight the topological surface states inside the bulk gap. (D) The surface Dirac cone near \bar{M} . The Fermi surface is shown with a helical spin texture.

shown in Figs. 1C and D, exhibit a simple Dirac-cone-like energy dispersion. The Dirac cone starts warping at higher energies due to the cubic symmetry of the lattice. The Fermi surface below the Dirac point exhibits a right-hand helical “spin”-texture on the top surface, similar to that of Bi_2Se_3 -type TI materials [23], while the helicity corresponds to angular momenta $m_j = \pm 1/2$, instead of real electron spin. The Fermi velocity near the Dirac point is estimated to be approximately 0.75×10^5 m/s, and inside the large bulk energy gap, the TSSs are well localized on the surface atomic layers to about two BBO units or around 1 nm in thickness. On the other hand, to obtain the minimal effective model of the band topology, we derive a four-band Hamiltonian similar to that for Bi_2Se_3 [24] in the basis of $|p; j = 1/2, m_j = +1/2 \rangle$, $|s; j = 1/2, m_j = +1/2 \rangle$, $|p; j = 1/2, m_j = -1/2 \rangle$, and $|s; j = 1/2, m_j = -1/2 \rangle$:

$$H(\mathbf{k}) = \epsilon_0(\mathbf{k})\mathbb{I}_{4 \times 4} + \begin{pmatrix} \mathcal{M}(\mathbf{k}) & Ak_z & 0 & Ak_- \\ Ak_z & -\mathcal{M}(\mathbf{k}) & Ak_- & 0 \\ 0 & Ak_+ & \mathcal{M}(\mathbf{k}) & -Ak_z \\ Ak_+ & 0 & -Ak_z & -\mathcal{M}(\mathbf{k}) \end{pmatrix} \quad (1)$$

where $\mathbf{k} = \mathbf{k}_0 - \mathbf{k}_R$ (0.5, 0.5, 0.5) is centred at the R point, and $k_{\pm} = k_x \pm ik_y$, $\epsilon_0(\mathbf{k}) = C + Dk^2$, and $\mathcal{M}(\mathbf{k}) = M - Bk^2$. The main difference from that of the Bi_2Se_3 Hamiltonian is that Eq. 1 is isotropic to \mathbf{k} due to the cubic symmetry. We obtain the parameters of Eq. 1 by fitting the energy spectrum of the effective Hamiltonian to that of the *ab initio* calculations for the electron-doped cubic BBO using $M = -0.625$ eV, $A = 2.5$ eVÅ, $B = -9.0$ eVÅ², and $D = 1.5$ eVÅ². Subsequently, the Fermi

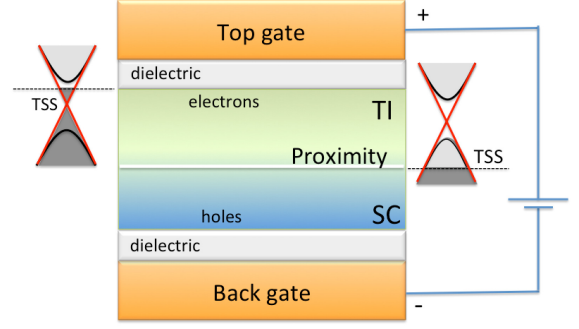


FIG. 2: Schematic illustration of the interface between the topological insulator (TI) and superconducting (SC) state in a gated thin film device. The top and bottom surfaces are the TI and SC regions, respectively. The position of the Fermi energy (dashed lines) shifts down in the band structure. In the middle region, topological surface states (TSSs) are interfaced with SC states and become SC due to the proximity effect.

velocity of the TSSs is given by $v = A/\hbar \simeq 0.5 \times 10^5$ m/s, which is consistent with the *ab initio* calculations.

We can confirm that the TI phase is stable against lattice distortions. The monoclinic BBO band structure (Fig. 1B) shows that the R point of the cubic lattice is projected onto the Γ point due to band folding, but the s - p band inversion at this Γ point is still present and the indirect gap is unchanged (0.7 eV). Since the inversion strength (the energy difference between the $|s, j = 1/2 \rangle$ and $|p, j = 1/2 \rangle$ bands) is nearly 2 eV (1.2 eV for the electron-doped structure), the TI phase is not destroyed by the O-breathing or -tilting distortions. Furthermore, band structure calculations using the hybrid functional method [5, 6], which is known to treat the dynamical correlation effect well for BBO [15, 27], also validated the inversion for both the ideal cubic and distorted structures. (Details are described in the Supplementary Information.)

Experimentally, electron-doped BBO may be achieved in $\text{BaBi}(\text{O}_{0.67}\text{F}_{0.33})_3$ by substituting O with F atoms. The O and F atom have comparable atomic radii and electronegativities, which can keep the octahedral BiO_6 stable. For example, F substitution for O was applied for iron-based superconductor LaOFeAs to realize electron-doping [29]. It is also possible to employ a state-of-art electrolyte gating technique to BBO to induce heavy electron-doping, which was realized for several mixed-valent compounds [30–32]. In addition, oxygen vacancies, which are commonly observed in experiments [33], are also natural electron donors in $\text{BaBiO}_{3-\delta}$. On the other hand, although the TSSs are unoccupied in pristine BBO compounds, it may be possible to monitor these states directly via monochromatic two-photon photoemission, as was recently employed to monitor the empty TSSs of Bi chalcogenides [34].

Thus far we can state that BBO becomes a superconductor with hole doping and a potential TI with electron doping. If *pn*-junction-type devices are fabricated with BBO, an interface between the TSSs and the superconductor may be realized, which is necessary for the realization of Fu and Kane's [12] proposal on Majorana Fermions for quantum computation. Here, we outline a double-gated thin-film configuration, as illustrated in Fig. 2. If the bottom and top regions of the film are pre-doped as *p* and *n* type, respectively, the double-gated structure may feasibly induce a hole-rich bottom surface and an electron-rich top surface, resulting in TSSs and superconductivity states on the top and bottom surfaces, respectively. In the middle region of the slab, the TSSs overlap with the bulk bands and penetrate the bulk. These TSSs can then become superconducting as a result of the proximity effect with the bottom superconducting regime. Such a structure is likely to be attainable as high-quality BBO thin films, which have been successfully grown on SrTiO₃ [35–37] and MgO [37] substrates. And moreover, the O-tilting lattice distortion was recently found to be suppressed in a BBO(001) thin film on MgO [37], which is very close to our required cubic structure.

The band structure of BaBiO₃ can act as a prototype for designing new perovskite TIs. Ba can be substituted by Sc, Y, or La to obtain new compounds as analogues of an electron-doped BBO. We found in calculations that a similar band inversion exists in this case. However, these compounds are semimetals (the Sc/Y/La-*d* orbitals are lower in energy than the Bi-*p* states) and induce topological semimetals. In contrast, CsTlCl₃-type halide perovskites, which are predicted to be superconductor candidates [4–6], have band structures that are similar to BBO. However, we did not observe *s*-*p* inversion for ATlX₃ (X = Cs, Rb, F, Cl, Br, or I), because the SOC of Tl is not strong enough. When we can substitute Tl with Sn or Pb, we find that heavier members of this family, such as CsSnI₃ and CsPbI₃, are near the boundary of a topological trivial–nontrivial phase transition. Compressive pressure is necessary to drive these boundary materials into the TI region, which is consistent with recent theoretical calculations of these halides [38].

We thank Prof. X.-L. Qi at Stanford University and Prof. S. S. P. Parkin at IBM Almaden Research Center San Jose for fruitful discussions. B.Y. acknowledges financial support from the ERC Advanced Grant (291472) and computing time at HLRN Berlin/Hannover (Germany).

* Electronic address: yan@cpfs.mpg.de

- [1] Sleight, A. W., Gillson, J. L. & Bierstedt, P. E. High-temperature superconductivity in the BaPb_{1-x}Bi_xO₃ systems. *Solid State Comm.* **17**, 27–28 (1975).
- [2] Cava, R. J. *et al.* Superconductivity near 30 K without copper: the Ba_{0.6}K_{0.4}BiO₃ perovskite. *Nature* **332**, 814–816 (1988).
- [3] Yin, Z. P., Kutevov, A. & Kotliar, G. Correlation enhanced electron-phonon coupling and high temperature superconductivity. *arXiv:1110.5751* (2011).
- [4] Yin, Z. P. & Kotliar, G. Rational material design of mixed-valent high-T_c superconductors. *Europhys. Lett.* **101**, 27002 (2013).
- [5] Retuerto, M. *et al.* Synthesis and properties of the theoretically predicted mixed-valent perovskite superconductors: CsTlX₃ (X = F, Cl). *arXiv:1302.2353* (2013).
- [6] Schoop, L. M., Muehler, L., Felser, C. & Cava, R. J. Lone Pair Effect, Structural Distortions and Potential for Superconductivity in TI Perovskites. *arXiv:1302.1785* (2013).
- [7] Qi, X. & Zhang, S. The quantum spin hall effect and topological insulators. *Physics Today* **63**, 33 (2010).
- [8] Moore, J. The birth of topological insulators. *Nature* **464**, 194–198 (2010).
- [9] Hasan, M. Z. & Kane, C. L. Colloquium: Topological insulators. *Rev. Mod. Phys.* **82**, 3045–3067 (2010).
- [10] Qi, X.-L. & Zhang, S.-C. Topological insulators and superconductors. *Rev. Mod. Phys.* **83**, 1057 (2011).
- [11] Yan, B. & Zhang, S.-C. Topological materials. *Rep. Prog. Phys.* **75**, 096501 (2012).
- [12] Fu, L. & Kane, C. L. Superconducting proximity effect and majorana fermions at the surface of a topological insulator. *Phys. Rev. Lett.* **100**, 096407 (2008).
- [13] Cox, D. E. & Sleight, A. W. Crystal structure of Ba₂Bi³⁺Bi⁵⁺O₆. *Solid State Comm.* **19**, 969–973 (1976).
- [14] Mattheiss, L., Gyorgy, E. & Johnson, D. Superconductivity above 20 K in the Ba-K-Bi-O system. *Phys. Rev. B* **37**, 3745–3746 (1988).
- [15] Khan, Y., Nahm, K., Rosenberg, M. & Willner, H. Superconductivity and semiconductor–metal phase transition in the system BaPb_{1-x}Bi_xO₃. *Phys. Status Solidi A* **39**, 79–88 (1977).
- [16] Pei, S. *et al.* Structural phase diagram of the Ba_{1-x}K_xBiO₃ system. *Phys. Rev. B* **41**, 4126–4141 (1990).
- [17] Mattheiss, L. & Hamann, D. Electronic structure of BaPb_{1-x}Bi_xO₃. *Phys. Rev. B* **28**, 4227–4241 (1983).
- [18] Vielsack, G. & Weber, W. Search for negative U in the Ba_{1-x}K_xBi_{1-y}Pb_yO₃ system using constrained density-functional theory. *Phys. Rev. B* **54**, 6614–6623 (1996).
- [19] Meregalli, V. & Savrasov, S. Electron-phonon coupling and properties of doped BaBiO₃. *Phys. Rev. B* **57**, 14453–14469 (1998).
- [20] Bernevig, B. A., Hughes, T. L. & Zhang, S. C. Quantum spin hall effect and topological phase transition in hgte quantum wells. *Science* **314**, 1757 (2006).
- [21] König, M. *et al.* Quantum spin hall insulator state in hgte quantum wells. *Science* **318**, 766–770 (2007).
- [22] Fu, L. & Kane, C. L. Topological insulators with inversion symmetry. *Phys. Rev. B* **76**, 045302 (2007).
- [23] Hsieh, D. *et al.* A tunable topological insulator in the spin helical dirac transport regime. *Nature* **460**, 1101–1105 (2009).
- [24] Zhang, H. *et al.* Topological insulators in Bi₂Se₃, Bi₂Te₃ and Sb₂Te₃ with a single Dirac cone on the surface. *Nature Phys.* **5**, 438–442 (2009).
- [25] Heyd, J., Scuseria, G. E. & Ernzerhof, M. Erratum: “Hy-

- brid functionals based on a screened Coulomb potential” [J. Chem. Phys. 118, 8207 (2003)]. *J. Chem. Phys.* **124**, 219906–219906–1 (2006).
- [26] Krukau, A. V., Vydrov, O. A., Izmaylov, A. F. & Scuseria, G. E. Influence of the exchange screening parameter on the performance of screened hybrid functionals. *J. Chem. Phys.* **125**, 224106 (2006).
- [27] Franchini, C., Kresse, G. & Podloucky, R. Polaronic Hole Trapping in Doped BaBiO₃. *Phys. Rev. Lett.* **102** (2009).
- [28] Franchini, C., Sanna, A., Marsman, M. & Kresse, G. Structural, vibrational, and quasiparticle properties of the Peierls semiconductor BaBiO₃: A hybrid functional and self-consistent GW+vertex-corrections study. *Phys. Rev. B* **81** (2010).
- [29] Kamihara, Y., Watanabe, T., Hirano, M. & Hosono, H. Iron-Based Layered Superconductor LaO_{1-x}F_xFeAs ($x = 0.050.12$) with T_c = 26 K. *J. Am. Chem. Soc.* **130**, 3296–3297 (2008).
- [30] Ye, J. T. *et al.* Liquid-gated interface superconductivity on an atomically flat film. *Nature Materials* **9**, 125–128 (2009).
- [31] Jeong, J. *et al.* Suppression of Metal-Insulator Transition in VO₂ by Electric Field-Induced Oxygen Vacancy Formation. *Science* **339**, 1402–1405 (2013).
- [32] Nakano, M. *et al.* Collective bulk carrier delocalization driven by electrostatic surface charge accumulation. *Nature* **487**, 459–462 (2012).
- [33] Suzuki, M. & Murakami, T. Effect of oxygen vacancies on carrier localization in BaPb_{1-x}Bi_xO₃. *Solid State Comm.* **53**, 691–694 (1985).
- [34] Niesner, D. *et al.* Unoccupied topological states on bismuth chalcogenides. *Phys. Rev. B* **86** (2012).
- [35] Sato, H., Tajima, S., Takagi, H. & Uchida, S. Optical study of the metal-insulator transition on Ba_{1-x}K_xBiO₃ thin films. *Nature* **338**, 241–243 (1989).
- [36] Gozar, A., Logvenov, G., Butko, V. & Bozovic, I. Surface structure analysis of atomically smooth BaBiO₃ Films. *Phys. Rev. B* **75** (2007).
- [37] Inumaru, K., Miyata, H. & Yamanaka, S. Partial suppression of structural distortion in epitaxially grown BaBiO₃ thin films. *Phys. Rev. B* **78** (2008).
- [38] Jin, H., Im, J. & Freeman, A. J. Topological insulator phase in halide perovskite structures. *Phys. Rev. B* **86** (2012).

Supplementary Information

Method

In band structure calculations, we employed *ab initio* density-functional theory (DFT) with the generalized gradient approximation (GGA) [1]. We employed the *Vienna ab initio simulation package* with a plane wave basis [2]. The core electrons were represented by the projector-augmented-wave potential [3]. For hybrid-functional calculations, we adopted HSE06 [4–6] exchange-correlation functional and interpolated the band structures using Wannier functions [7], where the DFT wavefunctions were projected to Bi-*sp*, Ba-*d* and O-*p* orbitals. The cubic crystal structure of BaBiO₃(BBO)

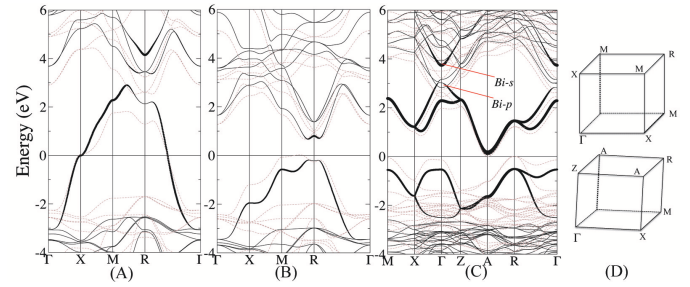


FIG. 3: Band structures of BBO calculated with HSE06 functionals for (A) ideal cubic, (B) electron-doped cubic (with lattice expansion), and (C) monoclinic structures. The thickness of black lines indicate the contribution of Bi-*s* states. Results from GGA are also shown with brown dashed lines. SOC is only included for cubic lattices in A and B, but not for the monoclinic lattice in C. (D) The first Brillouin zones are shown for the cubic (up) and monoclinic (down) lattices.

was taken from ref. [8] with lattice constant $a = 4.35$ Å and the monoclinic structure was from ref. [9].

Band structures of BBO with hybrid-functionals

We validated the band structures of both cubic and monoclinic lattices using HSE06 functionals. For the cubic lattice, spin-orbit coupling (SOC) was also included. Compared to GGA, HSE06 was found to shift both the conduction and valence bands (see Figs. S1A and B), consist with ref. [10]. One can see clearly that the Bi-5*s* state is still above the energy gap, perserving the *s* – *p* band inversion. From Fig.1 of the paper, SOC can dramatically modify the Bi-6*p* bands, while it does not change the Bi-*s* band. Therefore, the *s* – *p* inversion will remain when SOC exists, if they are already inverted without SOC. Without SOC a clear feature of *s* – *p* inversion is the *p*-state degeneracy at the *R* point right above the Fermi energy (Fig. 1A of the paper). In many previous literatures that did not employ SOC, actually, this feature can be clearly observed [10–14]. So we performed HSE06 calculations without SOC for the monoclinic lattice, in order to reduce the computational time of large supercells. Our result agrees with recent HSE06 calculations [15]. In Fig. S1C, one can also see the *s* – *p* inversion. In all, we conclude that the band inversion is robust with hybrid-functionals for both ideal cubic and distorted lattices.

Band structures of ABiO₃(A=Sc, Y and La)

We calculated GGA band structures of ABiO₃(A=Sc, Y and La). The *s* – *p* band inversion exists for all three compounds, in which the Fermi energy shifts into the

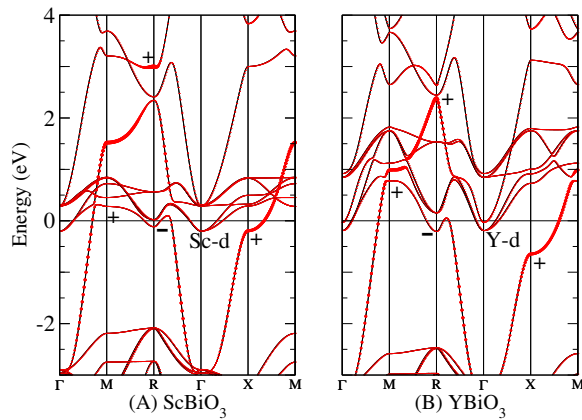


FIG. 4: Band structures of bulk ScBiO_3 and YBiO_3 calculated with GGA. Red balls present bands with Bi-s states. Parities are labeled.

inversion gap (See the band structures of ScBiO_3 and YBiO_3 for exmaples in Fig. S2). Therefore, they have the same nontrivial topological Z_2 invairants (1;1,1,1). However, the Sc/Y-d states exhibit lower energy than Bi-p states, resulting in a zero indirect gap. So these compounds are topological semimetals. In addition, we optimized the lattice constants of the perovskite lattice as 4.35, 4.41, and 4.46 Å for Sc, Y and La compounds, respectively, before calculating band structures.

* Electronic address: yan@cpfs.mpg.de

- [1] Perdew, J. P., Burke, K. & Ernzerhof, M. Generalized gradient approximation made simple. *Phys. Rev. Lett.* **77**, 3865 (1996).
- [2] Kresse, G. & Hafner, J. Ab initio molecular dynamics for liquid metals. *Phys. Rev. B* **47**, 558–561 (1993).
- [3] Kresse, G. & Joubert, D. From ultrasoft pseudopotentials to the projector augmented-wave method. *Phys. Rev. B*

- 59**, 1758–1775 (1999).
- [4] Heyd, J., Scuseria, G. E. & Ernzerhof, M. Hybrid functionals based on a screened Coulomb potential. *J. Chem. Phys.* **118**, 8207–8215 (2003).
- [5] Heyd, J., Scuseria, G. E. & Ernzerhof, M. Erratum: “Hybrid functionals based on a screened Coulomb potential” [*J. Chem. Phys.* 118, 8207 (2003)]. *J. Chem. Phys.* **124**, 219906–219906–1 (2006).
- [6] Krukau, A. V., Vydrov, O. A., Izmaylov, A. F. & Scuseria, G. E. Influence of the exchange screening parameter on the performance of screened hybrid functionals. *J. Chem. Phys.* **125**, 224106 (2006).
- [7] Mostofi, A. A. *et al.* wannier90: A tool for obtaining maximally-localised Wannier functions. *Comput. Phys. Commun.* **178**, 685–699 (2008).
- [8] Cox, D. E. & Sleight, A. W. Mixed-valent $\text{Ba}_2\text{Bi}_3+\text{B}_5+\text{O}_6$: structure and properties vs temperature. *Acta Crystallogr. Sect. B* **35**, 1–10 (1979).
- [9] Cox, D. E. & Sleight, A. W. Crystal structure of $\text{Ba}_2\text{Bi}_3+\text{Bi}_5+\text{O}_6$. *Solid State Comm.* **19**, 969–973 (1976).
- [10] Yin, Z. P., Kutepov, A. & Kotliar, G. Correlation enhanced electron-phonon coupling and high temperature superconductivity. *arXiv:1110.5751* (2011).
- [11] Mattheiss, L. & Hamann, D. Electronic structure of $\text{BaPb}_{1-x}\text{Bi}_x\text{O}_3$. *Phys. Rev. B* **28**, 4227–4241 (1983).
- [12] Takegahara, K. Electronic band structures in cubic perovskite-type oxides: bismuthates and transition metal oxides. *J. Electron. Spectrosc. Relat. Phenom.* **66**, 303–320 (1994).
- [13] Vielsack, G. & Weber, W. Search for negative U in the $\text{Ba}_{1-x}\text{K}_x\text{Bi}_{1-y}\text{Pb}_y\text{O}_3$ system using constrained density-functional theory. *Phys. Rev. B* **54**, 6614–6623 (1996).
- [14] Korotin, D., Kukolev, V., Kozhevnikov, A. V., Novoselov, D. & Anisimov, V. I. Electronic correlations and crystal structure distortions in BaBiO_3 . *J. Phys: Condens. Matter* **24**, 415603 (2012).
- [15] Franchini, C., Sanna, A., Marsman, M. & Kresse, G. Structural, vibrational, and quasiparticle properties of the Peierls semiconductor BaBiO_3 : A hybrid functional and self-consistent GW+vertex-corrections study. *Phys. Rev. B* **81** (2010).